Evaluation of ORR Active Sites in Nitrogen-doped Carbon Nanofibers by KOH Post Treatment

Navaneethan Muthuswamy,[a] Marthe E. M. Buan,[a] John C. Walmsley,[b] and Magnus Rønning*[a]

[a] Department of Chemical Engineering, Norwegian University of Science and Technology, 7491 Trondheim, Norway

[b] SINTEF Materials and Chemistry, Høgskoleringen 5, 7465 Trondheim, Norway

Keywords

Nitrogen-doped carbon; Carbon nanofiber; KOH treatment; Carbon electrocatalysis; Oxygen reduction reaction; Active site

Abstract

Oxygen reduction on N-doped carbon nanomaterials is believed to take place at either N-centered active sites (C-N_x) or Fe-centered active sites (Fe-N_x). In this work the origin of the oxygen reduction on nitrogen-doped carbon nanofibers (N-CNFs) is investigated by removing nitrogen and iron from the N-CNF surface using high temperature KOH treatment. The activities for the oxygen reduction reaction (ORR) in 0.5M H_2SO_4 are correlated with the XPS results and discussed with respect to the contribution from C-N_x and Fe-N_x active sites. Increasing the time and temperature of the KOH treatment decreased the iron and nitrogen content at the N-CNF surface. The contribution from Fe-N_x active sites was found to be minor compared to the C-N_x active sites as the KOH-treated N-CNFs with no iron in the surface still showed considerable ORR activity. Furthermore, the activity was maintained when the fraction of pyridinic-N was greatly reduced compared to quaternary-N. Finally, even when no iron or nitrogen could be detected by XPS, 50 % of the initial oxygen reduction activity of the N-CNFs persisted. It is therefore suggested that there are active sites not originating from iron or nitrogen atoms, but rather from a distinct carbon environment.

* Corresponding author. E-mail: magnus.ronning@ntnu.no

1 Introduction

Developing novel, highly active, and cheap catalysts for the oxygen reduction reaction (ORR) in acidic electrolyte is crucial to take the PEM fuel cell technology to market [1–4]. In this objective, several new catalytic materials have recently been developed through rational design, and shown promising catalytic performance for the oxygen reduction [4–6]. One of the most promising materials is nitrogen doped carbon nanomaterials prepared in the presence of Fe, hereafter called Fe-N-C, which have opened a new opportunity to replace the costly Pt-based catalysts currently used [7–13]. However, a PEM fuel cell assembled with state-of-the-art Fe-N-C catalysts generate lower current density than the state-of-the-art Pt-based catalysts [2]. In turn, this increases the capital cost for the Fe-N-C fuel cell stack as the required electrode area increases, thereby increasing the requirements of other fuel cell components such as the bipolar plates. Lowering the capital cost of the Fe-N-C fuel cell can be achieved if the number of active sites in the Fe-N-C catalysts is increased so that higher current densities can be obtained. In this case it is important to perform fundamental studies to identify the key active site for the ORR on Fe-N-C catalysts and find suitable synthesis conditions to achieve more active sites.

Substantial efforts have recently been made to determine the key active sites on Fe-N-C catalysts using sophisticated instruments. Two main active sites have been hypothesized; one consisting of non-metallic sites in a carbon graphitic structure (C-N_x) and another consisting of an active metal center stabilized by nitrogen ligands (Fe-N_x) [5,14–20].

In C-N_x, nitrogen doping could lead to unique electron-donor nitrogen-atom-centered active sites [21–23]. In addition, the nitrogen can modify the electronic density of the adjacent carbon atoms creating electron-acceptor carbon-atom-centered active sites [8,24–26]. This will introduce electrophilic and nucleophilic character to the surface, and consequently affect the interaction with oxygen and intermediate reaction products [8,27]. Various types of nitrogen-groups are found in N-doped carbon nanomaterials with the three most common types being pyridinic, pyrrolic and quaternary nitrogen [23,26,28,29]. It has been proposed that the presence of pyridinic nitrogen on graphitic edge planes may be playing a more important role for the ORR activity compared to the other nitrogen groups [23,28].

For Fe-N_x active sites it is believed that the Fe atom coordinated to nitrogen atoms plays an important role in the oxygen reduction reaction. The Fe atom can be involved directly in the ORR by facilitating O_2 adsorption [30–32], or it functions as a bi-functional active site by providing favorable reaction intermediates for the ORR. However, some studies have

suggested that Fe is not directly involved in the ORR, but merely facilitates the growth of N-doped carbon with a distinct microstructure or surface chemistry suitable for oxygen reduction [5,18,28,33–35]. The presence of carbon edges has been found to be beneficial for the oxygen reduction without contribution from any dopant or metal atoms [36][37]. First principle calculations have shown that defects in CNT or graphene surfaces activate the adsorption and dissociation of O_2 [38][39]. Chu et al. reported a correlation between oxygen reduction and the amount of edge sites in carbon fibers [40].

Several research groups have deliberately poisoned their Fe-N-C catalysts with carbon monoxide, cyanide and sulphur to determine whether Fe is present in the active site for the oxygen reduction [41,42]. The poisoning experiments were based on evidence that Fe-porphyrins (Fe-N_4) have higher affinity for CO or CN^- than for oxygen [41]. However, the attempts of deactivating the Fe-N-C catalyst were unsuccessful. For Ozkan's research group no difference was observed in the linear sweep voltammetry (LSV) in O_2-saturated electrolyte and in an electrolyte with a mixture of O_2 and CO showing that the active site was totally inert to any interaction with CO.

In this work, we have deliberately removed both nitrogen and iron from our Fe-N-C catalyst by KOH and subsequent H_2SO_4 treatment to investigate the involvement of C-N_x and Fe-N_x active sites for the oxygen reduction reaction.

2 Experimental

2.1 Synthesis and KOH treatment

Nitrogen-doped carbon nanofibers supported on expanded graphite (EG) were prepared following the same method as described in previous reports [12,13]. In brief, the growth catalyst (0.5-0.5g, 20wt% Fe/EG) was loaded in the reactor and reduced in an H_2/Ar flow (40/160 ml/min, 5.0/5.0, AGA) while heating the furnace up to 650°C. Subsequently, N-CNFs were grown at 650°C using a synthesis gas mixture of CO/NH_3/H_2 (150/6.5/20 ml/min, 3.7/3.6/5.0, AGA). The synthesis time was 44 hours giving a total weight of 2.2g N-CNF/EG after synthesis.

Alkaline treatment was performed by grinding the N-CNF sample (0.4 g) with KOH pellets (1.6 g) and ethanol (96%). The mixture was then placed on a stainless-steel holder and loaded into a vertical reactor. To remove air present in the reactor, Ar was flushed for 30min before the N-CNF/KOH mixture was heated at 10ºC/min to 800ºC or 900ºC in Ar. The temperature was kept for 30 or 60min before cooling the reactor to room temperature. Thereafter the

samples were washed with 1M H_2SO_4 (95-97% H_2SO_4, Sigma Aldrich), DI-water and ethanol, and dried at 100 ºC overnight. Subsequently, a heat treatment in Ar for 1h at 900ºC was employed to remove excess oxygen groups introduced on the surface. The obtained samples were named "800KOH-0.5h", "800KOH-1.0h" and "900KOH-0.5h" indicating the temperature and duration of the KOH treatment.

2.2 Physicochemical characterization

The specific surface area of the N-CNFs was calculated by the Brunauer-Emmet-Teller (BET) method from N_2-adsorption measurements performed in a Micromeritics TriStar II 3020. The specific pore volume (2-300 nm) was obtained by Barret-Joyner-Halenda analysis of the desorption isotherm and the specific micropore volume was determined using the t-plot model.

The microstructure and morphology of the N-CNFs was observed using a Hitachi S-5500 scanning transmission electron microscope (S(T)EM). Transmission electron microscopy (TEM) using a Jeol JEM-ARM200F was employed to characterize the nanostructure of the N-CNFs. Both the S(T)EM and TEM samples were prepared by dispersing N-CNFs in isopropanol by ultra-sonication. A drop of the dispersion was then deposited on a holey carbon film supported by a copper grid and dried at room temperature.

X-ray photoelectron spectroscopy (XPS) measurements were carried out in a Kratos Axis Ultra DLD spectrometer using monochromatic Al Kα radiation (hν = 1486.58 eV). Sample preparation was done by covering carbon tape with an even layer of catalyst powder. Survey spectra were collected using fixed analyzer pass energies of 160 eV while the high-resolution spectra were collected at pass energies of 20 eV. Data analysis was performed using the CasaXPS software. The elemental composition was calculated after the subtraction of Shirley-type backgrounds for the high-resolution spectra. The N 1s region was deconvoluted using Gaussian-Lorentzian line shapes with 30% Lorentzian weighting.

2.3 Electrochemical characterization

The electrochemical characterization was conducted in a conventional three-electrode setup using a reversible hydrogen electrode (RHE) as reference electrode and a platinum wire as counter electrode. All potentials reported in this paper are given versus the RHE. A rotating ring disk electrode (RRDE, disk: 5 mm ϕ, ring: Pt with 20 % collection efficiency) was used as working electrode. The N-CNF catalysts were deposited on the glassy carbon disk electrode using the method described by Schmidt et al. [43]. The catalyst suspension was prepared by

sonicating 3.0 mg of N-CNFs in a mixture of 500 µL Millipore H_2O, 200 µL ethanol (100%), 200 µL isopropanol and 100 µL of 0.5 wt% Nafion® (DuPont™ DE521, Ion Power,Inc) for one hour. About 16 µL of the suspension was placed on the glassy carbon disk and dried under a N_2-flow giving approximately 245 µg/cm^2 of N-CNF catalyst on the electrode surface.

Before performing ORR the electrolyte was saturated with Ar and the electrodes were cleaned using cyclic voltammetry between 1.2 V and 0 V at different scanning rates. The background current was then measured by linear sweep voltammetry (LSV) from 1.10 V to 0.01 V at 5 mVs^{-1} in the Ar-saturated electrolyte. Oxygen reduction experiments were carried out in O_2-saturated 0.5M H_2SO_4 (95-97% H_2SO_4, Sigma Aldrich) at room temperature. The potential range of the ORR was 1.10 V - 0.01 V, the scan rate 5 mVs^{-1} and the rotational speed 1600 rpm. The third cathodic scan after background subtraction is reported for all catalysts. Onset potentials for the oxygen reduction (E_{ORR}) were determined by comparing the LSV curve obtained in Ar with the ORR measurement.

In order to detect the amount of H_2O_2 produced on the working electrode during the ORR, a constant potential of 1.2 V vs. RHE was applied to the Pt ring electrode. The H_2O_2 yield was calculated from the ring current (I_R), the disk current (I_D) and the collection efficiency of the Pt ring (N) using the following equation [44]:

$$H_2O_2\ (\%) = 200 \times \frac{(I_R / N)}{(I_R / N) + I_D} \qquad (1)$$

3 Results and discussion

Treatment of the N-CNFs with KOH was performed at high temperatures (800 and 900ºC) for 30 or 60 minutes. Following a cleaning and drying procedure, the samples were heat treated once more to remove oxygen functional groups introduced by the KOH. Only characterization of the N-CNFs after both heat treatment steps will be presented. To indicate the temperature and duration of the KOH treatment the N-CNFs are named “800KOH-0.5h”, “800KOH-1.0h” and “900KOH-0.5h” after treatment.

3.1 Structure and porosity

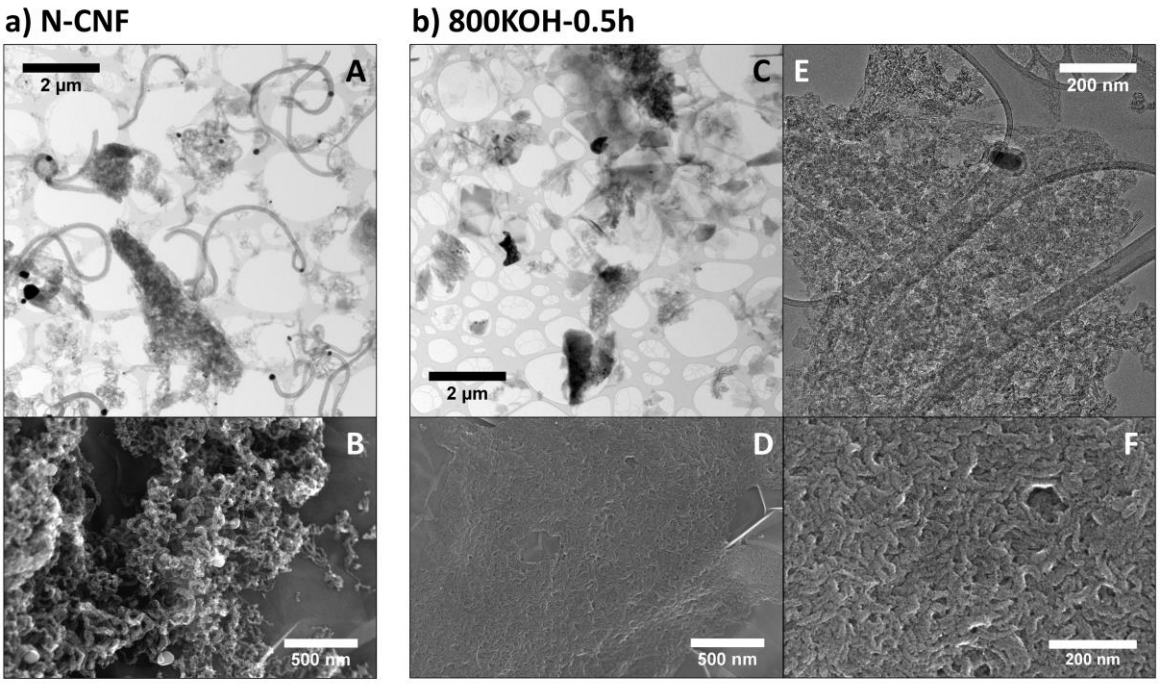

Figure 1 *TEM (A,C,E) and SEM (B,D,F) images of as-synthesized N-CNFs (**a**) and N-CNFs treated in KOH at 800°C for 0.5h (**b**).*

SEM and TEM images of the as-prepared N-CNFs on graphite and KOH treated counterparts are shown in Fig. 1a and 1b respectively. The as-prepared N-CNFs consist of well dispersed, loosely bound and ordered crystalline fibers. Whereas in the case of KOH treated N-CNFs, the fibrous shape was collapsed and aggregated to form compact layers. This structural change was also observed by Seong-Ho Yoon et al [45] in KOH treated un-doped CNFs. It has been proposed that partial gasification of the carbon by the products formed *in-situ* from KOH decomposition expands the interlayer spacing between graphene planes of the CNFs. This is followed by the destruction of the fibrous structure by a potassium intercalation and de-intercalation process. The proposed mechanism was supported by X-ray diffraction, SEM and TEM studies.

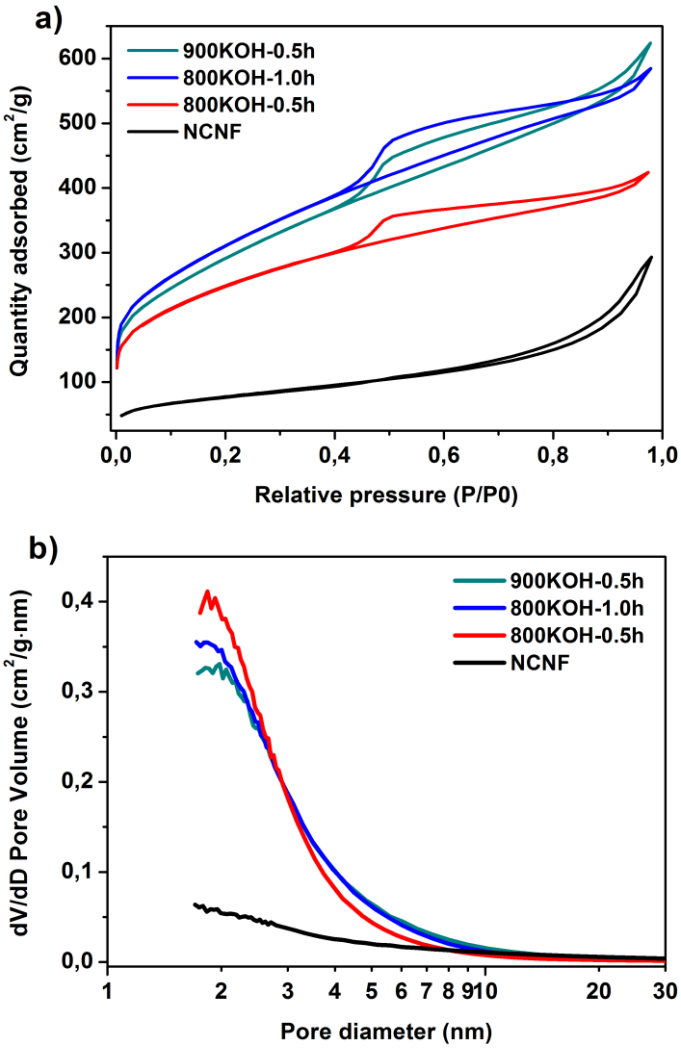

Figure 2 *Nitrogen adsorption isotherms for N-CNFs and KOH-treated N-CNFs (**a**) along with the pore distribution obtained from BJH of the adsorption isotherm (**b**).*

Nitrogen adsorption-desorption isotherms of the as-prepared and KOH treated N-CNFs are shown in Fig. 2a. All samples, including the pristine N-CNFs, show a hysteresis loop in the higher pressure region. This is due to the capillary condensation of N_2 gas molecules on pre-adsorbed multilayer N_2 molecules, and indicates the presence of mesopores in all the samples. Furthermore, the shape of the hysteresis loop represents nearly the hysteresis type H_3, according to IUPAC's classification of hysteresis loops. The H_3 type isotherm is observed in samples exhibiting wide capillaries with narrow openings or an interstice between the parallel planes [46].

The occurrence of a more pronounced hysteresis loop with KOH treatment indicates an increase in the amount of mesopores. This was supported by the pore size distribution (PSD) obtained from BJH of the adsorption isotherm, Fig. 2b, where an increase in pores with diameter 2 - 5 nm was observed after KOH treatment. The adsorption isotherm was used to

calculate the PSD since the desorption isotherm is more prone to be affected by pore network effects [47]. The mesopores in the KOH treated samples may have formed from either introduction of new mesopores or from the aggregation of N-CNFs as seen in the SEM images D and F in Fig. 1b. Moreover, there was a sharp initial uptake in the lower pressure region of the N_2 isotherm. This is characteristic of micropore filling of N_2 gas molecules and reveals the presence of pores below 2 nm. It is suggested that the etching of the carbon framework with KOH proceeds as $6KOH + 2C \rightarrow 2K + 3H_2 + 2K_2CO_3$, followed by the reaction of K_2CO_3 with carbon directly or through the decomposed product K_2O to form CO [48]. The metallic K intercalates into the carbon matrix during the activation and is removed during washing leaving a porous network in the carbon material.

To some extent macropores, type II isotherm, should also be present as no saturation limit was observed. This could stem from graphene sheet folding of the expanded graphite which was used as a growth catalyst support to grow N-CNFs.

In summary, the surface area, the adsorption capacity and porosity of the N-CNFs/EG composite was significantly increased by increasing the temperature for KOH treatment. Micropores and sub-mesopores should have been introduced in both N-CNFs and expanded graphite. The BET and BJH analysis (Table 1) shows that both the specific surface area and pore volume increased from 270 m^2/g and 0.424 cm^3/g for N-CNFs to 1151 m^2/g and 0.787 cm^3/g for 800KOH-1.0h.

3.2 Elemental composition

Table 1 *Elemental composition obtained by XPS analysis of the N-CNFs along with the results from the nitrogen adsorption measurements.*

Sample	**N** ***(at%)***	**O** ***(at%)***	**Fe** ***(at%)***	**BET** ***(m^2/g)***	**V_{pores}** ***(cm^3/g)***	**V_{micro}** ***(cm^3/g)***
NCNF	4.7	1.4	0.24	270	0.424	0.021
800KOH-0.5h	0.5	1.4	0.02	878	0.560	0.053
800KOH-1.0h	0.3	1.2	NA	1151	0.787	0.023
900KOH-0.5h	NA	0.8	NA	1050	0.880	0.006

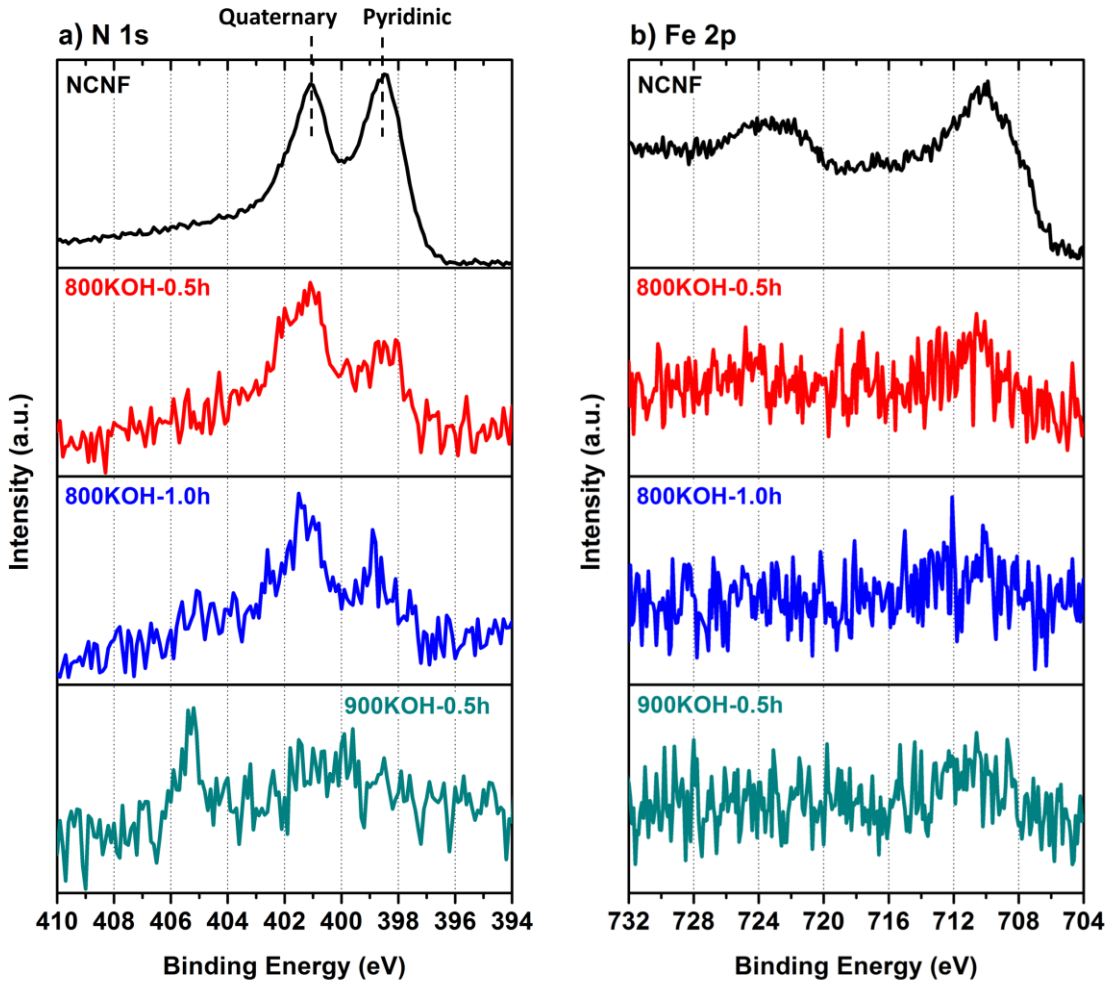

Figure 3 *High resolution XPS before and after KOH-treatment and annealing of the N-CNFs showing (**a**) N 1s region and (**b**) Fe 2p region.*

Nitrogen and iron were efficiently removed from the N-CNFs by KOH treatment. Table 1 shows how the elemental composition in the surface of the N-CNFs changed with time and temperature of the KOH treatment. The nitrogen and iron contents were 4.7at% and 0.24at% respectively before treatment and drastically decreased to only 0.5at% N and 0.02at% Fe after the mildest KOH-treatment (800ºC, 0.5h). Thereafter the level of Fe and N in the surface of the N-CNF/EG decreased gradually with increasing time and temperature of the KOH treatment. For the sample 900KOH-0.5h no iron or nitrogen could be detected by XPS analysis.

Most of the nitrogen was present as pyridinic-N (36%, 398.4eV) and quaternary-N (32%, 401eV) in the pristine N-CNFs as observed from Figure 3a. Upon KOH treatment, the peak intensity for pyridinic-N dropped significantly more than the peak intensity for quaternary-N for the N-CNFs treated at 800ºC. This is in good agreement with previous studies where quaternary-N was found to be more stable than pyridinic-N [49,50]. However, the peak for

both quaternary-N and pyridinic-N disappears completely for the sample treated at 900ºC. It is expected that the decomposed product K_2O originating from the KOH redox reaction with carbon could react with the N-CNFs and form NO and CO.

XPS analysis of the Fe 2p peak, Figure 3b, shows that the iron in the as-obtained N-CNFs is present as a mixture of Fe^0 and Fe-oxides. The peak intensity for Fe 2p diminishes and becomes unnoticeable when increasing the temperature for KOH treatment. The TEM images in Figure 1 show that iron nanoparticles were present both in the tip and in the middle of the N-CNFs before treatment. After KOH and subsequent acid treatment the amount of iron particles was significantly reduced, although some iron particles could still be observed. However, the remaining particles were encapsulated in several layers of carbon and were not detected by XPS. The low Fe 2p signal after treatment indicated that no iron was left in the surface of the N-CNFs.

3.3 Oxygen Reduction Reaction

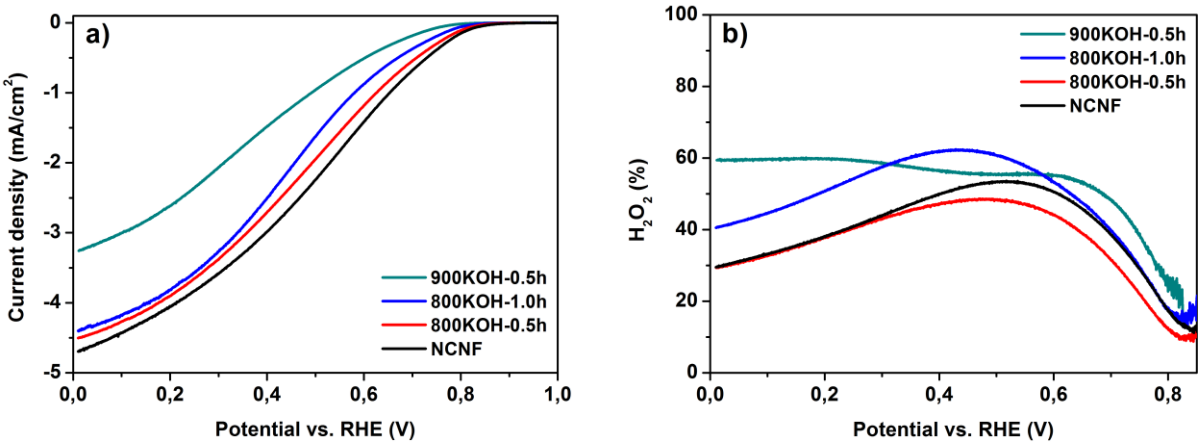

Figure 4 *(**a**) Oxygen reduction in 0.5M H_2SO_4 of the N-CNFs before and after KOH-treatment and annealing. (**b**) Corresponding amount of H_2O_2 detected with a Pt ring during the ORR. The catalyst loading was 245 µg/cm^2 and the polarization curves were acquired at 5mV/s and 1600rpm.*

All the N-CNF catalysts were tested for the oxygen reduction reaction in 0.5M H_2SO_4 electrolyte and the results are presented in Figure 4. The activity for the samples treated at 800ºC for 0.5h and 1.0h decreased moderately, while the ORR activity of the N-CNFs treated at 900ºC decreased drastically. Although most of the iron and nitrogen was removed by the KOH-treatment (Table 1), the 800KOH-0.5h sample still showed almost similar ORR activity

as the pristine N-CNFs. It appears that the majority of the nitrogen and iron initially present in the N-CNFs was not contributing to the ORR activity of the N-CNFs.

In addition, more of the pyridinic-N was removed relative to the quaternary-N for the N-CNFs treated at 800ºC for 0.5h (Figure 3). This is not in agreement with previous studies where it has been proposed that pyridinic-N groups present at graphitic edge planes are more important for the ORR activity of N-doped carbon compared to quaternary-N [51]. The role of pyridinic-N could thus be linked to the stronger ability of edge planes to chemisorb oxygen atom. Conversely, this effect is unlikely in the present work since pyridinic-N was preferentially removed by KOH-treatment. Complete selective removal of the pyridinic-N groups is needed to confirm this. By carefully selecting KOH post treatment time and temperature the contribution from different nitrogen groups on the ORR activity can be exposed.

The sample treated at 800ºC for 1.0h showed no Fe-signal in the XPS analysis (Figure 2b), but the oxygen reduction activity still did not decrease severely compared to the pristine N-CNFs. This raises a controversy about the contribution of Fe centered active sites (Fe-N_x) for the ORR in N-CNFs. Figure 4 shows that there is some decrease in ORR current between 800KOH-0.5h and 800KOH-1.0h which contain 0.02at% and 0at% Fe respectively. In addition, the amount of H_2O_2 increased 10-15% at low overpotentials for 800KOH-1.0h compared to 800KOH-0.5h. This suggests there is a contribution from Fe to the ORR-activity for 800KOH-0.5h and that these Fe-sites are improving the selectivity towards the 4-electron oxygen reduction pathway. It is likely that some Fe centers are remaining in the N-CNFs treated at 800ºC for 1h, but that they were below the detection limit of the XPS. The contribution from Fe-N_x active sites to the ORR activity must however be minor when considering the relatively high catalytic activity of 800KOH-1.0h.

In any case, the ORR current decreased more significantly when neither nitrogen nor iron could be detected by XPS as was the case for the N-CNFs treated at 900ºC for 0.5h. This demonstrates that the nitrogen centered active sites (C-N_x) plays a predominant role for the oxygen reduction on N-CNFs. It is also interesting to note that the oxygen reduction activity is maintained reasonably high even when there is no considerable XPS signal observed for both nitrogen and iron. This indicates the presence of another active site not originating from Fe or nitrogen atoms, but rather from a distinct carbon environment formed during the N-CNFs synthesis in the presence of Fe catalysts.

The increase in surface area and pore volume after KOH-treatment could positively contribute to the ORR activity by increasing the accessibility of O_2 to more active sites.

However, for the sample treated at 900ºC the oxygen reduction activity decreased drastically while the surface area and amount of mesopores was comparable to the 800ºC samples (Table 1). This indicates that even if the increase in pore structure improved the oxygen redution activity to some extent, it cannot be the sole reason for the ORR activity of the KOH-treated N-CNFs.

4 Conclusion

KOH treatment was used to remove nitrogen and iron which are assumed to be responsible for the oxygen reduction activity of N-CNFs. XPS analysis showed that treating the N-CNFs with KOH at high temperatures efficiently removed N and Fe from the surface. Increasing the time or temperature of the treatment resulted in more nitrogen and iron being removed. Almost 90 % of the Fe-content and 91 % of the N-content in the pristine N-CNFs were found to be removed for the sample treated at 800°C for 0.5h. Most of the nitrogen left was present as quaternary-N, while the fraction of pyridinic-N was greatly reduced. However, the activity was much like the pristine N-CNFs. When the treatment time was increased to 1h the Fe-content in the surface was below the XPS detection limit, while the ORR activity only decreased moderately. The catalytic activity decreased significantly in the sample treated at 900°C when no nitrogen was detected. However, about 50 % of the ORR activity was maintained even when apparently all N and Fe was removed from the N-CNFs. It is therefore suggested that there are active sites not originating from iron or nitrogen atoms in the N-CNFs, but rather from a distinct carbon environment formed during the N-CNFs synthesis.

Acknowledgements

Financial support for this work was provided by the Norwegian University of Science and Technology (NTNU) and by the European Commision 7th Framework Programme (FP7) through the FREECATS project (grant no. 280658). The TEM work was carried out at the NORTEM Gemini Centre at NTNU and supported by the NORTEM project (grant no. 197405) within the INFRASTRUCTURE program of the Research Council of Norway (RCN). The RCN is also acknowledged for the support to the Norwegian Micro- and Nano-Fabrication Facility, NorFab.

References

[1] Y. Nie, L. Li, Z. Wei, Recent advancements in Pt and Pt-free catalysts for oxygen reduction reaction, Chem. Soc. Rev. (2015) 2168–2201. doi:10.1039/C4CS00484A.

[2] D. Bokach, S. ten Hoopen, N. Muthuswamy, M.E.M. Buan, M. Rønning, Nitrogen-doped carbon nanofiber catalyst for ORR in PEM fuel cell stack: Performance, durability and market application aspects, Int. J. Hydrogen Energy. 41 (2016) 17616–17630. doi:10.1016/j.ijhydene.2016.07.137.

[3] J.S. Spendelow, D.C. Papageorgopoulos, Progress in PEMFC MEA Component R&D at the DOE Fuel Cell Technologies Program, Fuel Cells. 11 (2011) 775–786. doi:10.1002/fuce.201000189.

[4] M. Shao, Q. Chang, J.-P. Dodelet, R. Chenitz, Recent Advances in Electrocatalysts for Oxygen Reduction Reaction, Chem. Rev. 116 (2016) 3594–3657. doi:10.1021/acs.chemrev.5b00462.

[5] Z. Chen, D. Higgins, A. Yu, L. Zhang, J. Zhang, A review on non-precious metal electrocatalysts for PEM fuel cells, Energy Environ. Sci. 4 (2011) 3167. doi:10.1039/c0ee00558d.

[6] C.R. Raj, A. Samanta, S.H. Noh, S. Mondal, T. Okajima, T. Ohsaka, Emerging new generation electrocatalysts for the oxygen reduction reaction, J. Mater. Chem. A. 4 (2016) 11156–11178. doi:10.1039/C6TA03300H.

[7] L. Yang, N. Larouche, R. Chenitz, G. Zhang, M. Lefèvre, J.-P. Dodelet, Activity, Performance, and Durability for the Reduction of Oxygen in PEM Fuel Cells, of Fe/N/C Electrocatalysts Obtained from the Pyrolysis of Metal-Organic-Framework and Iron Porphyrin Precursors, Electrochim. Acta. 159 (2015) 184–197. doi:10.1016/j.electacta.2015.01.201.

[8] K. Gong, F. Du, Z. Xia, M. Durstock, L. Dai, Nitrogen-Doped Carbon Nanotube Arrays with High Electrocatalytic Activity for Oxygen Reduction, Science (80-.). 323 (2009) 760–763.

[9] L. Qu, Y. Liu, J. Baek, L.D. Ќ, Nitrogen-Doped Graphene as Efficient Metal-Free Electrocatalyst for Oxygen Reduction in Fuel Cells, ACS Nano. 4 (2010) 1321–1326.

[10] F. Jaouen, E. Proietti, M. Lefèvre, R. Chenitz, J.-P. Dodelet, G. Wu, H.T. Chung, C.M. Johnston, P. Zelenay, Recent advances in non-precious metal catalysis for oxygen-reduction reaction in polymer electrolyte fuel cells, Energy Environ. Sci. 4 (2011) 114. doi:10.1039/c0ee00011f.

[11] A. Serov, K. Artyushkova, E. Niangar, C. Wang, N. Dale, F. Jaouen, M.-T. Sougrati, Q. Jia, S. Mukerjee, P. Atanassov, Nano-structured non-platinum catalysts for automotive fuel cell application, Nano Energy. 16 (2015) 293–300. doi:10.1016/j.nanoen.2015.07.002.

[12] M.E.M. Buan, N. Muthuswamy, J.C. Walmsley, D. Chen, M. Rønning, Nitrogen-doped carbon nanofibers on expanded graphite as oxygen reduction electrocatalysts, Carbon,. 101 (2016) 191–202. doi:10.1016/j.carbon.2016.01.081.

[13] M.E.M. Buan, N. Muthuswamy, J.C. Walmsley, D. Chen, M. Rønning, Nitrogen-doped Carbon Nanofibers for the Oxygen Reduction Reaction: Importance of Iron Growth Catalyst Phase, ChemCatChem. (2017). doi:10.1002/cctc.201601585.

[14] J. Herranz, F. Jaouen, M. Lefèvre, U.I. Kramm, E. Proietti, J.-P. Dodelet, P. Bogdanoff, S. Fiechter, I. Abs-Wurmbach, P. Bertrand, T.M. Arruda, S. Mukerjee, Unveiling N-Protonation and Anion-Binding Effects on Fe / N / C Catalysts for O 2 Reduction in Proton-Exchange-Membrane Fuel Cells, J. Phys. Chem. C. 115 (2011) 16087–16097.

[15] D. Singh, J. Tian, K. Mamtani, J. King, J.T. Miller, U.S. Ozkan, A comparison of N-containing carbon nanostructures (CNx) and N-coordinated iron-carbon catalysts (FeNC) for the oxygen reduction reaction in acidic media, J. Catal. 317 (2014) 30–43. doi:10.1016/j.jcat.2014.05.025.

[16] G. Liu, X. Li, J.-W. Lee, B.N. Popov, A review of the development of nitrogen-modified carbon-based catalysts for oxygen reduction at USC, Catal. Sci. Technol. 1 (2011) 207. doi:10.1039/c0cy00053a.

[17] U.I. Kramm, J. Herranz, N. Larouche, T.M. Arruda, M. Lefèvre, F. Jaouen, P. Bogdanoff, S. Fiechter, I. Abs-Wurmbach, S. Mukerjee, J.-P. Dodelet, Structure of the catalytic sites in Fe/N/C-catalysts for O2-reduction in PEM fuel cells, Phys. Chem. Chem. Phys. 14 (2012) 11673. doi:10.1039/c2cp41957b.

[18] K. Strickland, E. Miner, Q. Jia, U. Tylus, N. Ramaswamy, W. Liang, M.-T. Sougrati, F. Jaouen, S. Mukerjee, Highly active oxygen reduction non-platinum group metal electrocatalyst without direct metal–

nitrogen coordination, Nat. Commun. 6 (2015) 7343. doi:10.1038/ncomms8343.

[19] A. Zitolo, V. Goellner, V. Armel, M.-T. Sougrati, T. Mineva, L. Stievano, E. Fonda, F. Jaouen, Identification of catalytic sites for oxygen reduction in iron- and nitrogen-doped graphene materials, Nat. Mater. 14 (2015) 937–942. doi:10.1038/nmat4367.

[20] K. Mamtani, U.S. Ozkan, Heteroatom-Doped Carbon Nanostructures as Oxygen Reduction Reaction Catalysts in Acidic Media: An Overview, Catal. Letters. 145 (2014) 436–450. doi:10.1007/s10562-014-1434-y.

[21] K.N. Wood, R. O'Hayre, S. Pylypenko, Recent progress on nitrogen/carbon structures designed for use in energy and sustainability applications, Energy Environ. Sci. 7 (2014) 1212. doi:10.1039/c3ee44078h.

[22] T. Schiros, D. Nordlund, L. Pálová, D. Prezzi, L. Zhao, K.S. Kim, U. Wurstbauer, C. Gutiérrez, D. Delongchamp, C. Jaye, D. Fischer, H. Ogasawara, L.G.M. Pettersson, D.R. Reichman, P. Kim, M.S. Hybertsen, A.N. Pasupathy, Connecting Dopant Bond Type with Electronic Structure in N-Doped Graphene, Nano Lett. 12 (2012) 4025–4031. doi:10.1021/nl301409h.

[23] P. Matter, L. Zhang, U. Ozkan, The role of nanostructure in nitrogen-containing carbon catalysts for the oxygen reduction reaction, J. Catal. 239 (2006) 83–96. doi:10.1016/j.jcat.2006.01.022.

[24] Z. Yang, H. Nie, X. Chen, X. Chen, S. Huang, Recent progress in doped carbon nanomaterials as effective cathode catalysts for fuel cell oxygen reduction reaction, J. Power Sources. 236 (2013) 238–249. doi:10.1016/j.jpowsour.2013.02.057.

[25] X. Zou, Y. Zhang, Noble metal-free hydrogen evolution catalysts for water splitting, Chem. Soc. Rev. 44 (2015) 5148–5180. doi:10.1039/C4CS00448E.

[26] H. Wang, T. Maiyalagan, X. Wang, Review on Recent Progress in Nitrogen-Doped Graphene: Synthesis, Characterization, and Its Potential Applications, ACS Catal. 2 (2012) 781–794. doi:10.1021/cs200652y.

[27] D. Chen, A. Holmen, Z. Sui, X. Zhou, Carbon mediated catalysis: A review on oxidative dehydrogenation, Chinese J. Catal. 35 (2014) 824–841. doi:10.1016/S1872-2067(14)60120-0.

[28] P.H. Matter, U.S. Ozkan, Non-metal catalysts for dioxygen reduction in an acidic electrolyte, Catal. Letters. 109 (2006) 115–123. doi:10.1007/s10562-006-0067-1.

[29] N.P. Subramanian, X. Li, V. Nallathambi, S.P. Kumaraguru, H. Colon-Mercado, G. Wu, J.W. Lee, B.N. Popov, Nitrogen-modified carbon-based catalysts for oxygen reduction reaction in polymer electrolyte membrane fuel cells, J. Power Sources. 188 (2009) 38–44. doi:10.1016/j.jpowsour.2008.11.087.

[30] C.E. Szakacs, M. Lefèvre, U.I. Kramm, J.-P. Dodelet, F. Vidal, A density functional theory study of catalytic sites for oxygen reduction in Fe/N/C catalysts used in H_2 /O_2 fuel cells., Phys. Chem. Chem. Phys. 16 (2014) 13654–61. doi:10.1039/c3cp55331k.

[31] E.F. Holby, G. Wu, P. Zelenay, C.D. Taylor, Structure of Fe-Nx-C Defects in Oxygen Reduction Reaction Catalysts from First Principles Modeling, J. Phys. Chem. C. (2014) 140606130633002. doi:10.1021/jp503266h.

[32] F. Gao, G.-L. Zhao, Z. Wang, D. Bagayoko, D.-J. Liu, Catalytic reaction on FeN4/C site of nitrogen functionalized carbon nanotubes as cathode catalyst for hydrogen fuel cells, Catal. Commun. 62 (2015) 79–82. doi:10.1016/j.catcom.2015.01.015.

[33] S. Maldonado, K.J. Stevenson, Influence of nitrogen doping on oxygen reduction electrocatalysis at carbon nanofiber electrodes, J. Phys. Chem. B. 109 (2005) 4707–4716. doi:10.1021/jp044442z.

[34] P.H. Matter, E. Wang, J.M.M. Millet, U.S. Ozkan, Characterization of the iron phase in CNx-based oxygen reduction reaction catalysts, J. Phys. Chem. C. 111 (2007) 1444–1450. doi:10.1021/jp0651236.

[35] E.J. Biddinger, D. von Deak, U.S. Ozkan, Nitrogen-Containing Carbon Nanostructures as Oxygen-Reduction Catalysts, Top. Catal. 52 (2009) 1566–1574. doi:10.1007/s11244-009-9289-y.

[36] L. Tao, Q. Wang, S. Dou, Z. Ma, J. Huo, S. Wang, L. Dai, Edge-rich and dopant-free graphene as a highly efficient metal-free electrocatalyst for the oxygen reduction reaction, Chem. Commun. 52 (2016) 2764–2767. doi:10.1039/C5CC09173J.

[37] X. Zhao, X. Zou, X. Yan, C.L. Brown, Z. Chen, G. Zhu, X. Yao, Defect-driven oxygen reduction reaction (ORR) of carbon without any element doping, Inorg. Chem. Front. 3 (2016) 417–421.

doi:10.1039/C5QI00236B.

[38] S. Jiang, Z. Li, H. Wang, Y. Wang, L. Meng, S. Song, J.C.S. Wu, S.C. Yen, W.F. Huang, L.C. Chen, M.C. Lin, K.H. Chen, D. Strmcnik, N.M. Markovic, V.R. Stamenkovic, Tuning nondoped carbon nanotubes to an efficient metal-free electrocatalyst for oxygen reduction reaction by localizing the orbital of the nanotubes with topological defects, Nanoscale. 6 (2014) 14262–14269. doi:10.1039/C4NR04658G.

[39] H. Zhao, C. Sun, Z. Jin, D.-W. Wang, X. Yan, Z. Chen, G. Zhu, X. Yao, Carbon for the oxygen reduction reaction: a defect mechanism, J. Mater. Chem. A. 3 (2015) 11736–11739. doi:10.1039/C5TA02229K.

[40] X. Chu, K. Kinoshita, Surface modification of carbons for enhanced electrochemical activity, Mater. Sci. Eng. B. 49 (1997) 53–60. doi:10.1016/S0921-5107(97)00100-1.

[41] D. von Deak, D. Singh, J.C. King, U.S. Ozkan, Use of carbon monoxide and cyanide to probe the active sites on nitrogen-doped carbon catalysts for oxygen reduction, Appl. Catal. B Environ. 113–114 (2012) 126–133. doi:10.1016/j.apcatb.2011.11.029.

[42] D. Singh, K. Mamtani, C.R. Bruening, T. Miller, U.S. Ozkan, Use of H 2 S to Probe the Active Sites in FeNC Catalysts for the Oxygen Reduction Reaction (ORR) in Acidic Media, (2014).

[43] T.J. Schmidt, H.A. Gasteiger, G.D. Stäb, P.M. Urban, D.M. Kolb, R.J. Behm, Characterization of High-Surface-Area Electrocatalysts Using a Rotating Disk Electrode Configuration, J. Electrochem. Soc. 145 (1998) 2354–2358. doi:10.1149/1.1838642.

[44] U. a. Paulus, T.J. Schmidt, H. a. Gasteiger, R.J. Behm, Oxygen reduction on a high-surface area Pt/Vulcan carbon catalyst: a thin-film rotating ring-disk electrode study, J. Electroanal. Chem. 495 (2001) 134–145. doi:10.1016/S0022-0728(00)00407-1.

[45] S.-H. Yoon, S. Lim, Y. Song, Y. Ota, W. Qiao, A. Tanaka, I. Mochida, KOH activation of carbon nanofibers, Carbon N. Y. 42 (2004) 1723–1729. doi:10.1016/j.carbon.2004.03.006.

[46] K. Kaneko, Determination of pore size and pore size distribution: 1. Adsorbents and catalysts, J. Memb. Sci. 96 (1994) 59–89. doi:10.1016/0376-7388(94)00126-X.

[47] J.C. Groen, L.A.. Peffer, J. Pérez-Ramírez, Pore size determination in modified micro- and mesoporous materials. Pitfalls and limitations in gas adsorption data analysis, Microporous Mesoporous Mater. 60 (2003) 1–17. doi:10.1016/S1387-1811(03)00339-1.

[48] Y. Zhu, S. Murali, M.D. Stoller, K.J. Ganesh, W. Cai, P.J. Ferreira, A. Pirkle, R.M. Wallace, K.A. Cychosz, M. Thommes, D. Su, E.A. Stach, R.S. Ruoff, Carbon-Based Supercapacitors Produced by Activation of Graphene, Science (80-.). 332 (2011) 1537–1541. doi:10.1126/science.1200770.

[49] Y. Chen, Q. Liu, J. Wang, Highly Porous Nitrogen-Doped Carbon Nanofibers as Efficient Metal-Free Catalysts toward the Electrocatalytic Oxygen Reduction Reaction, Nano Adv. (2016) 79–89. doi:10.22180/na174.

[50] L. Li, A. Manthiram, O- and N-Doped Carbon Nanowebs as Metal-Free Catalysts for Hybrid Li-Air Batteries, Adv. Energy Mater. 4 (2014) 1301795. doi:10.1002/aenm.201301795.

[51] M.P. Woods, E.J. Biddinger, P.H. Matter, B. Mirkelamoglu, U.S. Ozkan, Correlation Between Oxygen Reduction Reaction and Oxidative Dehydrogenation Activities Over Nanostructured Carbon Catalysts, Catal. Letters. 136 (2010) 1–8. doi:10.1007/s10562-010-0304-5.